PERFORMANCE, NAVIGATION AND CONTROL OF A SPINNING ELECTRODYNAMIC TETHER SYSTEM

J. Simón-Aznar, G. Sánchez-Arriaga, and B. Vatankhahghadim

Department of Aerospace Engineering
Universidad Carlos III de Madrid, 28911 Leganés, Spain
Email: jorge.simon, gonzalo.sanchez, behrad.vatankhahghadim @uc3m.es

ABSTRACT

As compared with electrodynamic tethers (EDTs) aligned with the local vertical, the performance of spinning EDTs depends weakly on the orbit inclination and are more favorable for deorbiting space debris at high-inclined orbits. This work studies the optimal orientation of the spin plane to maximize the deorbit performance. A semi-analytical model for the decay rate, valid for circular orbits and based on a dipole model for the geomagnetic field, is presented and used to find a simple relation between the spin plane angle and the orbit inclination. Optimal values for the motional electric field and the decay rate as a function of the inclination are found, as well as the control law for the electric current of the EDT. A good agreement is found between the results of the semi-analytical model and BETsMA v2.0 simulations.

Keywords: Electrodynamic Tether; Spinning Systems; Space Debris; De-orbiting; Optimal Orientation.

1. INTRODUCTION

The rapid growth of orbital missions has led to an increasingly congested space environment, creating concerns about safe and cost-effective access to near-Earth orbits. Among the various end-of-life disposal solutions considered in recent years, electrodynamic tethers (EDTs) have drawn particular attention because they enable propellant-less propulsion through the Lorentz force induced by the interaction between the tether current and the Earth's magnetic field.

Spinning EDTs offer several advantages compared to EDTs aligned along the local vertical. By utilizing centrifugal forces to create tension, they can operate effectively under higher current, avoiding the dynamic instabilities of EDTs along the local vertical [8] and achieving more flexible orbit maneuvers than purely hanging tethers [6] aligned with the local vertical. This feature is particularly appealing for debris-removal scenarios, where the high performance and adaptability of spinning EDTs can significantly shorten the deorbiting time. The fact that the EDT rotates is an extra degree of difficulty. The effects of this rotation on the dynamics and how it can be controlled have been the subject of study and interest in recent decades [3], as well as its application for possible solutions to space debris removal, such as the ElectroDynamic Debris Eliminator (EDDE) [7]. In fact, spinning EDTs have received recent attention. For instance, current control laws for orbital variations [5], and for the spin-up process [16] and collision avoidance strategies [4] have been proposed in recent works.

An open problem related to spinning EDTs is the selection of the orientation of the spin plane. In principle, such a plane is not invariant due to the action of different perturbations like the Lorentz and gravitational torques [3][15]. However, if the spinning angular velocity is very large as compared with the orbital angular velocity, or appropriate control laws for the tether current are implemented, such a plane can be kept constant. The objective of this work is to study and find the optimal orientation of the spin plane of EDTs in deorbiting missions.

The work is organized as follows. Section 2 presents a dynamic model for spinning EDTs orbiting in circular orbit. Section 3 studies the optimal orientation of the spin plane for deorbiting scenarios. The behavior of the motional electric field and the decay rate as a function of the orbit inclination for optimal spin-plane conditions is shown. Section 4 compares the semi-analytical results with simulations carried out with BETsMA v2.0 [10], a mission analysis software for EDTs. Finally, Sec. 5 summarizes the conclusions of the work.

2. DYNAMIC MODEL

2.1. Kinematic considerations

We consider a spacecraft of mass m_S –modeled as a point– attached to a straight EDT of length L and mass m_T, and to an end point mass m_B. The total mass of the system reads $M = m_S + m_T + m_B$. The EDT is bare, and captures electrons passively from the ambient

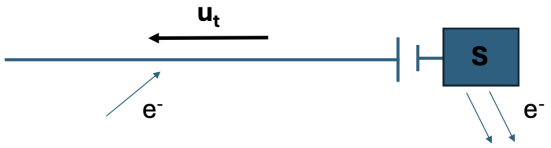

Figure 1. Sketch of an EDT with 1 cathode at the end mass S and the vector in the current direction $\boldsymbol{u_t}$.

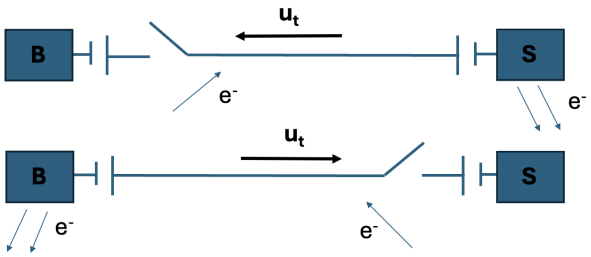

Figure 2. Sketch of an EDT with 2 cathodes, one in end mass S and one in end mass B, and the vector in the current direction $\boldsymbol{u_t}$.

plasma [11]. The electric circuit is closed with the ambient plasma by using cathodic contactors. Figures 1 and 2 shows two different systems with one and two cathodes, respectively.

For systems equipped with two cathodes, the current can flow in both directions depending on which cathode is active. The electric current along the tether is written as $\boldsymbol{I} = I(s)\boldsymbol{u}_t$, where s is the tether coordinate measured from the anodic point and $\boldsymbol{u}_t$ an unit vector along the tether direction. For a bare tether, the current profile $I(s)$ depends on tether design and ambient variables like the plasma density and the component of the motional electric field along $\boldsymbol{u}_t$, *i.e.*

$$E_m \equiv (\boldsymbol{v}_{rel} \times \boldsymbol{B}) \cdot \boldsymbol{u}_t \tag{1}$$

with $\boldsymbol{v}_{rel}$ the tether-to-plasma relative velocity [11]. Since involving $\boldsymbol{u}_t$, the value of E_m depends on the tether attitude, which is very important because the larger E_m the larger I_{av} for the same ambient conditions, such as the plasma density.

Once it is found, the average current along the tether is computed from

$$I_{av} = \frac{1}{L}\int_0^L I(s)ds \tag{2}$$

For convenience, the base $\{\boldsymbol{i}_I, \boldsymbol{j}_I, \boldsymbol{k}_I\}$ is used to denote the unit vectors along the axes of an inertial frame with its origin at the center of the Earth. The X_I-Y_I plane spans the equatorial plane, X_I points to the Aries point and Z_I is along the Earth's rotation axis.

Similarly, a body frame attached to the spinning tether is also defined and with its origin at the center of mass C_M of the tether system. The X_B-axis is along the vector $\overline{SB}$

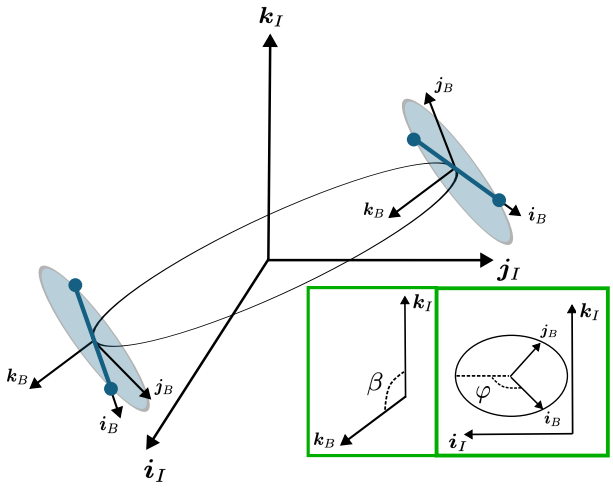

Figure 3. Sketch of a spinning EDT system with body and inertial frames.

–going from point S to point B–, and the Y_B and Z_B axes are normal to it. The unit vectors along these axes are

$$\boldsymbol{i}_B = \frac{\overline{SB}}{L}; \quad \boldsymbol{j}_B = \frac{d\boldsymbol{i}_B/dt}{|d\boldsymbol{i}_B/dt|}; \quad \boldsymbol{k}_B = \boldsymbol{i}_B \times \boldsymbol{j}_B \tag{3}$$

The angular velocity of the body frame with respect to the inertial frame is

$$\begin{aligned}\boldsymbol{\Omega}_{BI} &= \Omega_{\parallel}\boldsymbol{i}_B + \boldsymbol{\Omega}_{\perp} \equiv \Omega_{\parallel}\boldsymbol{i}_B + \boldsymbol{i}_B \times \frac{d\boldsymbol{i}_B}{dt} \\ &= \Omega_{\parallel}\boldsymbol{i}_B + |\frac{d\boldsymbol{i}_B}{dt}|\boldsymbol{k}_B \equiv \Omega_{\parallel}\boldsymbol{i}_B + \boldsymbol{\Omega}_{\perp}\end{aligned} \tag{4}$$

where Eq. (3) is employed. Therefore, the angular velocity has a component along the tether direction and another component along $\boldsymbol{k}_B$. We introduce the spin plane as the plane normal to $\boldsymbol{k}_B$ and the spin angle β as

$$\boldsymbol{\Omega}_{\perp} = -\sin\beta\boldsymbol{j}_I + \cos\beta\boldsymbol{k}_I \tag{5}$$

Then, the components in the inertial frame of the unit vector along the electric current reads

$$\boldsymbol{u_t} = \pm\frac{\overline{\boldsymbol{SB}}}{L} \equiv \pm(\cos\varphi\,\boldsymbol{i}_I + \sin\varphi\,[\cos\beta\,\boldsymbol{j}_I + \sin\beta\,\boldsymbol{k}_I]). \tag{6}$$

where φ is the in-plane angle measured from $\boldsymbol{i}_I$ and the plus (minus) sign should be taken if the active cathode is at point S (B). Figure 3 shows two examples of the direction vectors in the body frame with respect to the inertial frame and the angles in Eq. (6).

The third and last frame of reference is an orbital frame with its center at C_M.The X_O-axis points radially outward (local zenith), Z_O-axis is normal to the orbital plane, and the Y_O-axis is perpendicular to both and complete a right-handed frame. The unit vectors $\{\boldsymbol{i}_O, \boldsymbol{j}_O,$

$\boldsymbol{k}_O\}$ along these axes are

$$\boldsymbol{i}_O = \frac{\boldsymbol{r}}{|\boldsymbol{r}|}; \quad \boldsymbol{k}_O = \frac{\boldsymbol{r}\times\boldsymbol{v}}{|\boldsymbol{r}\times\boldsymbol{v}|}; \quad \boldsymbol{j}_O = \boldsymbol{k}_O \times \boldsymbol{i}_O \tag{7}$$

where $\boldsymbol{r}$ and $\boldsymbol{v}$ are the position and velocity vectors of the center of mass of the tether system.

2.2. Equation of Motion

It is assumed that the only perturbation is the Lorentz force acting on the bare EDT. In addition, the magnetic field $\boldsymbol{B}$ is assumed to be constant along the tether since the tether's length is small compared to the radius of the orbit. The Lorentz force then reads

$$\begin{aligned}\boldsymbol{F_L} &= \int_0^L I(s)\,\boldsymbol{u}_t \times \boldsymbol{B}\,ds \approx \boldsymbol{u}_t \times \boldsymbol{B}\int_0^L I(s)\,ds \\ &\equiv LI_{av}\,\boldsymbol{u}_t \times \boldsymbol{B}\end{aligned} \tag{8}$$

where Eq. (2) is used. This section, where a semi-analytical model is constructed, assumes that the Earth magnetic field is a dipole with center and axis at the center of the Earth and along its rotation axis, respectively. Taking into account that the position vector of C_M is $\boldsymbol{r} = r\boldsymbol{i}_O$, the magnetic field is given by

$$\boldsymbol{B}(r) = B_0\left(\frac{R_E}{r}\right)^3 [\boldsymbol{k}_I - 3(\boldsymbol{k}_I\cdot\boldsymbol{i}_O)\boldsymbol{i}_O] \tag{9}$$

with B_0 the magnetic dipole intensity and R_E the radius of the Earth.

The dynamics of the center of mass is governed by

$$M\frac{d\boldsymbol{v}}{dt} = -\frac{\mu_E M}{r^3}\boldsymbol{r} + LI_{av}\boldsymbol{u}_t \times \boldsymbol{B} \tag{10}$$

where μ_E is the Earth gravitational parameter. Assuming that the Lorentz force is small and the spacecraft follows a sequence of quasi-circular orbits, with $v \approx \sqrt{\mu_E/r}$, the dot product of Eq. (10) and $\boldsymbol{v}$ is [1, 14]

$$\frac{dH}{dt} \approx \frac{2(R_E+H)^2}{\mu_E}\frac{\boldsymbol{F}_L\cdot\boldsymbol{v}}{M} \tag{11}$$

The fastest de-orbiting is reached by maximizing the Lorentz power

$$W_L \equiv \boldsymbol{F}_L\cdot\boldsymbol{v} = -LI_{av}\,(\boldsymbol{v}\times\boldsymbol{B})\cdot\boldsymbol{u}_t \approx -E_m LI_{av} \tag{12}$$

where Eq. (1) is used and it is assumed that $v_{rel} \approx v$.

3. OPTIMAL SPIN PLANE

As pointed out in Refs. [12, 13], the motional electrical field E_m, and therefore the tether attitude given by $\boldsymbol{u}_t$, appears twice when computing the deorbiting performance (see Eq. (12)). Firstly, the average current I_{av} for a bare tether depends on the motional electric field component along the tether, $E_m \equiv (\boldsymbol{v}_{rel}\times\boldsymbol{B})\cdot\boldsymbol{u}_t$. The larger E_m, the larger I_{av}. In case E_m is small, an onboard power supply can be used to polarize the bare tether positively and capture enough electrons from the ambient plasma to generate the desired current. Secondly, the Lorentz power is proportional to E_m, as shown in Eq. (12). For this reason, the optimal tether attitude has been investigated in several works and EDTs aligned with the local vertical and with instantaneous optimal attitude [12, 13], as well as spinning EDTs (see Ref. [3] and therein), have been considered. In particular, the best performance is found for an EDT that satisfies at every instant that $\boldsymbol{u}_t \times (\boldsymbol{v}\times\boldsymbol{B}) = 0$ because it maximizes the figure of merit

$$\tilde{E}_m \equiv \frac{E_m}{vB_{eq}} \tag{13}$$

where B_{eq} is the magnetic field at the equator

$$B_{eq}(H) = B_0\left(\frac{R_E}{R_E+H}\right)^3 \tag{14}$$

Besides the case $\boldsymbol{i}_B = (\boldsymbol{v}\times\boldsymbol{B})\,/\,|\,\boldsymbol{v}\times\boldsymbol{B}\,|$, two other interesting cases are a tether aligned with the local vertical ($\boldsymbol{i}_B = \boldsymbol{r}/r$), and a tether normal to the orbital plane ($\boldsymbol{i}_B = \boldsymbol{r}\times\boldsymbol{v}/|\boldsymbol{r}\times\boldsymbol{v}|$). For circular orbits, the normalized motional electric field $\tilde{E}_m$ for these three interesting scenarios can be found by substituting the relations

$$\boldsymbol{r} = r\,(\cos\nu\boldsymbol{i}_I + \cos i\sin\nu\boldsymbol{j}_I + \sin i\sin\nu\boldsymbol{k}_I) \tag{15}$$

$$\boldsymbol{v} = v\,(-\sin\nu\boldsymbol{i}_I + \cos i\cos\nu\boldsymbol{j}_I + \sin i\cos\nu\boldsymbol{k}_I) \tag{16}$$

$$\begin{aligned}\boldsymbol{B} = B_0\Big(\frac{R_E}{r}\Big)^3\Big[&-\frac{3}{2}\sin i\sin(2\nu)\boldsymbol{i}_I \\ &-\frac{3}{2}\sin(2i)\sin^2\nu\boldsymbol{j}_I + \Big(1-3\sin^2 i\sin^2\nu\Big)\boldsymbol{k}_I\Big]\end{aligned} \tag{17}$$

in Eq. (13), where ν is the true anomaly. For instance, for a tether with the optimal attitude, i.e. $\boldsymbol{i}_B$ parallel to $\boldsymbol{v}\times\boldsymbol{B}$, one finds the simple results

$$\boldsymbol{i}_B = \frac{\cos i\cos\nu\boldsymbol{i}_I + (1-3\sin^2 i)\sin\nu\boldsymbol{j}_I + \frac{3}{2}\sin 2i\sin\nu\boldsymbol{k}_I}{\sqrt{\cos^2 i\cos^2\nu + (1+3\sin^2 i)\sin^2\nu}} \tag{18}$$

$$\tilde{E}_m = B_0\Big(\frac{R_E}{r}\Big)^3\Big(\frac{\mu_E}{r}\big[\cos^2 i\cos^2\nu + (1+3\sin^2 i)\sin^2\nu\big]\Big)^{1/2} \tag{19}$$

One can also find the perpendicular angular velocity that, for the optimal attitude reads,

$$\frac{\boldsymbol{\Omega}_\perp}{\Omega_\perp} \equiv \frac{\boldsymbol{i}_B\times d\boldsymbol{i}_B/dt}{|\boldsymbol{i}_B\times d\boldsymbol{i}_B/dt|} = \frac{-3\sin 2i\boldsymbol{j}_I + 2\left(1-3\sin^2 i\right)\boldsymbol{k}_I}{6|\sin i|\sqrt{1+\cos^2 i}} \tag{20}$$

Interestingly, $\boldsymbol{\Omega}_\perp$ has no component along the line of nodes and does not involve the true anomaly. This result suggests to consider the case of a spinning EDT that

rotates within a plane normal to the vector given in Eq. (20) because it reaches the optimal attitude once or twice per revolution if equipped with one or two cathodes. According to Eqs. (5) and (20), such a spinning EDT has the spin angle

$$\tan\beta = \frac{3\sin 2i}{2\left(1-3\sin^2 i\right)} \tag{21}$$

To study the performance of spinning EDTs, we introduce the average of $\tilde{E}_m$ as

$$\left\langle \tilde{E}_m \right\rangle = \frac{1}{4\pi^2}\int_0^{2\pi}\left[\int_0^{2\pi}\frac{|\,(\boldsymbol{v}\times\boldsymbol{B})\cdot\boldsymbol{u}_t\,|}{vB_{eq}}d\varphi\right]d\nu \tag{22}$$

where, for each point along the orbit (ν value), an average along all possible spinning directions is taken. The absolute value implicitly assumes that the tethered system is equipped with two cathodes. If it has only one cathode, one should set the function inside the integral equal to zero for φ values satisfying $(\boldsymbol{v}\times\boldsymbol{B})\cdot\boldsymbol{u}_t < 0$. For non-spinning EDT, Eq. (22) becomes

$$\left\langle \tilde{E}_m \right\rangle = \frac{1}{2\pi}\int_0^{2\pi}\frac{|\,(\boldsymbol{v}\times\boldsymbol{B})\cdot\boldsymbol{u}_t\,|}{vB_{eq}}d\nu \tag{23}$$

Figure 4 shows the ratio $<\tilde{E}_m>$ versus the orbit inclination for different EDT attitudes. The thin lines display the results for optimal ($\boldsymbol{i}_B = (\boldsymbol{v}\times\boldsymbol{B})\,/\,|\,\boldsymbol{v}\times\boldsymbol{B}\,|$), vertical ($\boldsymbol{i}_B = \boldsymbol{r}/r$), and horizontal ($\boldsymbol{i}_B = \boldsymbol{r}\times\boldsymbol{v}/|\boldsymbol{r}\times\boldsymbol{v}|$) EDT found in Ref. [12]. The two spinning EDTs proposed in this work are shown with solid thick lines. Unlike EDTs aligned with the local vertical, the performance of spinning EDTs depends weakly on the orbit inclination. For the single-cathode spinning EDT, it outperforms for high-inclined orbits, whereas the double-cathode spinning EDT is advantageous for mid- and high-inclined orbits.

Taking the average in the right-hand side of Eq. (11) as in Eq. (22), and using Eqs. (12) and (22) one finds the decay rate

$$\frac{dH}{dt} = -\frac{2LI_{av}}{M}\frac{<\tilde{E}_m>}{\sqrt{\mu_E}}\frac{B_0R_E^3}{\left(R_E+H\right)^{3/2}} \tag{24}$$

Figure 5 shows the decay rate versus the orbit inclination for the optimal attitude and spinning EDTs with one and two cathodes. Three orbital altitudes are shown and we considered the values $M = 100$ kg, $I_{av} = 1A$ and $L = 1km$. According to Eq. (24), $dH/dt \propto I_{av}L/M$. Therefore, the performance of other tether lengths, current levels, and spacecraft masses can be found from Figure 5.

4. NUMERICAL SIMULATIONS

Previous analysis, which provided useful results and insights, relies on several assumptions like non-tilted dipole

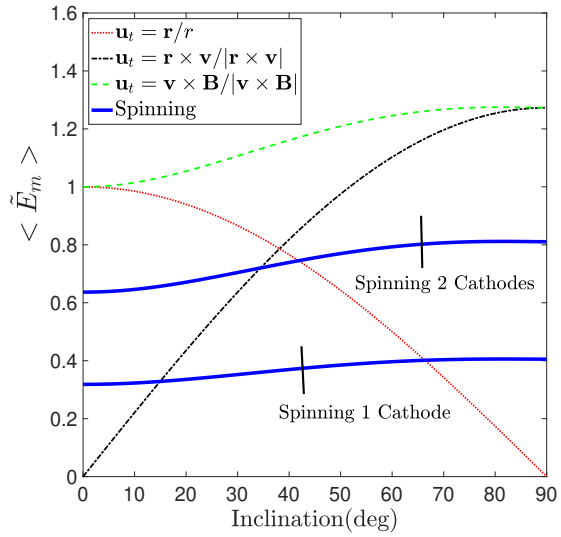

Figure 4. $<\tilde{E}_m>$ versus the orbit inclination for different tether attitudes. Results for optimal, vertical, and horizontal tethers are adapted from [12].

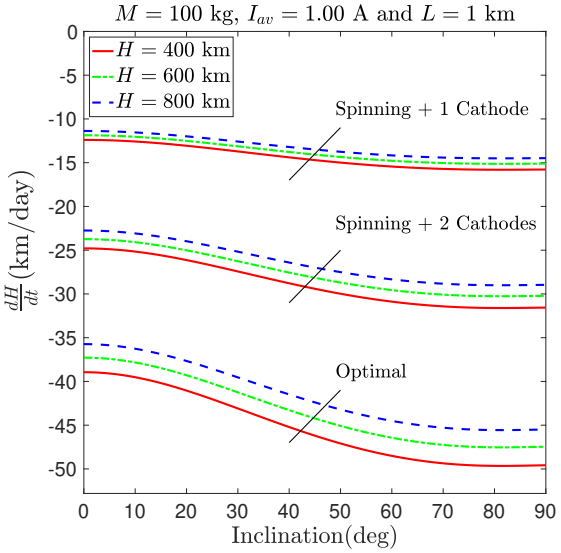

Figure 5. Decay rate versus orbit inclination for three orbital altitudes.

magnetic field, E_m averaged along one orbit and EDT revolution, etc. This section presents numerical simulations using the mission analysis software BETsMA v2.0 [10] to study the impact of such simplifying assumptions on the performance of the spinning EDT. The analysis is restricted to spinning EDTs with a single cathode, tether length 1 km, total system mass 100 kg and an initial orbit with zero eccentricity, altitude equal to of 600 km, vanishing right ascension of the ascending node. Unless the explicitly value for β is given, the orientation of the spin plane of the EDT was taken by using Eq. (21) for each orbit inclination. In the BETsMA v2.0 simulations, the tether's width and thickness were 2.5 cm and 50 μm respectively. The satellite was assumed to have enough available power (or a set of resistors) to keep the current at the cathode equal to 1 A. The EDT spin rate is constant and equal to 0.08 rpm, which corresponds to about 7 revolutions per orbit. The Earth's magnetic field and the plasma density were modeled by using the International Geomagnetic Reference Frame 11th (IGRF-11) [2] and the International Reference Ionosphere models, with the date set to January 3, 2014. Air drag and spherical harmonics due to gravity were not considered. BETsMA v2.0 uses the DROMO [9] orbital propagator with a Runge-Kutta numerical integrator. The stop condition for the simulations was one day.

4.1. Current Control Law

The software BETsMA v2.0 computes E_m taking into account all the environment variables given by the models IGRF-11 and IRI for the Earth's magnetic field and the ionosphere, in addition to a more realistic motion of the tether and the center of mass of the system. Therefore, it is expected from Eq. 1 that it presents variations of the motional electric field along one orbit.

Figure 6 shows the evolution of E_m (upper plot) and I_{av} (lower plot) in one orbit revolution for an inclination of 50° and the optimal angle of the spin plane β. The dashed line represents the results obtained with BETsMA v2.0 and it can be seen in the first plot that E_m effectively varies in time and shows a certain periodicity. According to the spin rate of about 7 revolutions per orbit, the same number of picks can be seen. In addition, when $E_m < 0$, I_{av} is set to zero since the Lorentz force opposes the desired variation (de-orbiting) and changes over time due to its dependence on E_m. The solid blue lines represent the results obtained with the semi-analytical model. The average current, unlike for BETsMA, is a constant that is fed directly into the Eq. (24) and, it is in Eq. (22) where the function inside the integrals is set to zero when its sign is negative. Therefore, to match the conditions between BETsMA v2.0 and the semi-analytical model, the average current of the latter is computed as the average of the positive values given by the software. The analytical intervals have been shown to be in agreement with the numerical values, underlining the effectiveness of the model used and supporting the conclusion that the prevailing current law weakly depends on the assumptions.

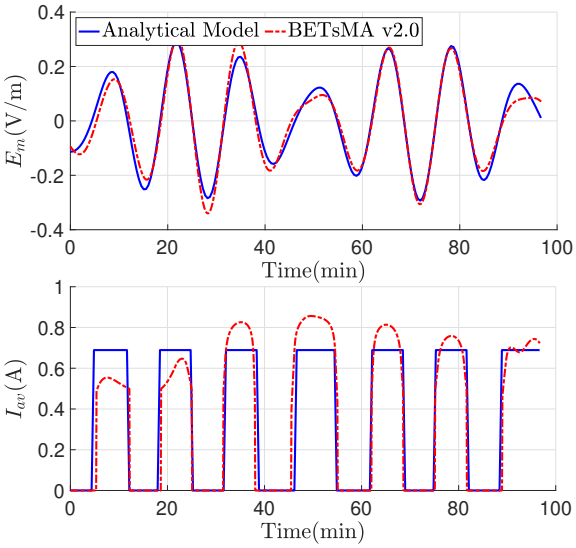

Figure 6. Evolution of the motional electric field E_m (a) and the average current I_{av} (b) over one orbit.

4.2. Optimal Angle

In this comparison, a variation in the optimal spin plane angle is introduced. The analysis is conducted for three inclination angles: $i = 0°, i = 50°$ and $i = 98°$. Each simulation produced a different average current, so the value of I_{av} in the analytical model was adjusted to match the corresponding result from the BETsMA v2.0 simulations.

The semi-analytical and numerical results for the optimal angle for the spin plane are displayed in Figure 7, where the normalized decay rate has been used to facilitate the comparison between the semi-analytical model results and the BETsMA v2.0 results. The optimal angle, *i.e.* the one that gives the maximum variation of the altitude, is shown to be the same for the equatorial and for the sun-synchronous orbits. For the mid-inclination orbit ($i = 50°$), the angles differ by approximately 2.5°. The decay altitude results obtained from the two approaches slightly differ for the optimal spinning planes, as shown in non-dimensional form in Figure 7. For equatorial, mid-inclination and sun-synchronous orbits, the differences are 707.05 m, 372.75 m and 130.02 m, respectively. These correspond to relative errors of 7.3%, 3.6% and 1.2%, respectively. The simulations by BETsMA v2.0 show the highest altitude variations.

5. CONCLUSIONS

Due to dynamic considerations, the most common tether attitudes considered in previous works are EDTs aligned with the local vertical and spinning EDTs. The selection of one solution or the other has strong consequences on many aspects of the EDT system, including the per-

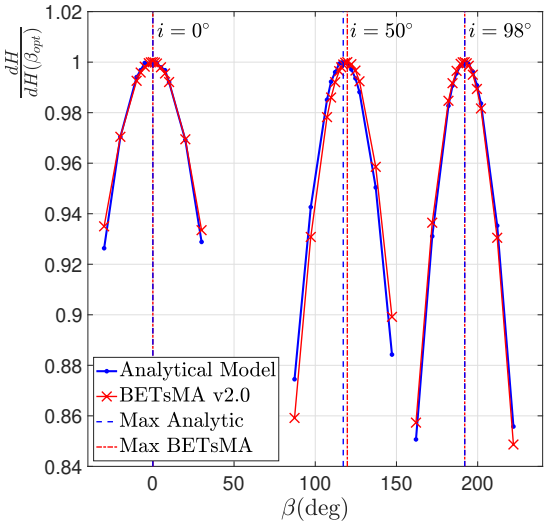

Figure 7. Optimal angle for the spin plane for three different inclinations: $i = 0°, i = 50°$ *and* $i = 98°$

formance. In deorbiting missions, the latter is measured by the decay rate, which is proportional to the motional electric field and the tether current. In turn, the latter is also proportional to E_m, which according to Eq. (1) is strongly dependent on the EDT attitude. Therefore, the selection of the appropriate tether attitude is critical.

The semi-analytical model that has been presented provides the decay rate for spinning EDTs and it highlights the weak dependence with the orbit inclination and their high efficiency in highly-inclined orbits as compared to EDTs aligned with the local vertical. One of the most important output of the model is an analytical formula for the angle β that orientates the spin plane with respect to the inertial frame. Such angle was determined by ensuring that, at least once per EDT revolution, the EDT is in the optimal orientation (tether parallel to the motional electric field). The results of the analytical formula, that relies in several simplifying assumptions, were compared with BETsMA v2.0 software's results. A good agreement was found for three representative orbit inclinations (equatorial, mid-latitude, and sun-synchronous). The relative errors between the analytical and the numerical simulations remained between about 1% and 7%, suggesting that proposed analytical formula is useful for preliminary mission design. The model also provides useful information about the required control law for the tether current. The variation of other orbital parameters, which can also be studied with the proposed model, will be presented elsewhere.

ACKNOWLEDGMENTS

This work was supported by the European Union's Horizon Europe Research and Innovation Program (No. 101161603, E.T.COMPACT project).

REFERENCES

1. Bombardelli, C., Zanutto, D., Lorenzini, E. (2013) Deorbiting Performance of Bare Electrodynamic Tethers in Inclined Orbits, *Journal of Guidance, Control, and Dynamics*, **36**(5), 1550–1556
2. Finlay, C. C., Maus, S., Beggan, C. D. *et al.* (2010) International Geomagnetic Reference Field: the eleventh generation, *Geophysical Journal International*, **183**(3), 1216–1230
3. Levin, E. M. (2007) *Dynamic Analysis of Space Tether Missions*, American Astronautical Society
4. Li, L., Li, A., Lu, H. *et al.* (2024) Collision-avoidance strategy for a spinning electrodynamic tether system, *Astrodynamics*, **8**(2), 247–259
5. Lu, H., Zabolotnov, Y. M., Li, A. (2019) Application of spinning electrodynamic tether system in changing system orbital parameters, *Journal of Physics: Conference Series*, **1368**
6. Pearson, J., Levin, E. M., Carroll, J. *et al.* (2004) Orbital Maneuvering With Spinning Electrodynamic Tethers, *2nd International Energy Conversion Engineering Conference*, **3**
7. Pearson, J., Levin, E. M., Carroll, J. *et al.* (2010) ElectroDynamic Debris Eliminator (EDDE): Design, Operation, and Ground Support
8. Peláez, J., Lorenzini, E.C., López-Rebollal, O. *et al.* (2000) A New Kind of Dynamic Instability in Electrodynamic Tethers, *Journal of the Astronautical Sciences*, **48**, 449–476
9. Peláez, J., Hedo, J. (2003) Un método de perturbaciones espaciales en dinámica de tethers, *Monografías de la Real Academia de Ciencias Exactas, Físicas, Químicas y Naturales de Zaragoza*, **22**, 119–140
10. Sánchez-Arriaga, G., Borderes-Motta, G., Chiabó, L. (2022). A code for the analysis of missions with electrodynamic tethers, *Acta Astronautica*, **198**, 471–481
11. Sanmartin, J. R., Martinez-Sanchez, M., Ahedo, E. (1993). Bare wire anodes for electrodynamic tethers, *Journal of Propulsion and Power*, **9**(3), 353–360
12. Sanmartin, J. R., Ahedo, E., Conde, L. *et al.* (2001). Short Electrodynamic Tethers, **476**, 581
13. Sanmartin, J. R., Ahedo, E. (2002). Trade-off Study on Deorbiting S/C in near Polar Orbit, *38th AIAA/ASME/SAE/ASEE Joint Propulsion Conference & Exhibit*
14. Sanmartin, J. R., Sánchez, A., Khan, S. B. *et al.* (2015). Optimum sizing of bare-tape tethers for deorbiting satellites at end of mission, *Advances in Space Research*, **56**(7), 1485–1492
15. Urrutxua, H., Peláez, J., Lara, M. (2012) Frozen orbits for scientific missions using rotating tethers, *Advances in the Astronautical Sciences*, **143**, 2475–2490
16. Wang, Y., Li, A., Lu, H. *et al.* (2025) Current Analysis and Optimal Control of a Spinning Bare Electrodynamic Tether System During its Spin-up Process, *Guidance, Navigation and Control*, **5**(01), 85–99